

1 Identifying plausible historical scenarios for coupled lake level
2 and seismicity rate changes: The case for the Dead Sea during
3 the last two millennia.

4 **Mariana Belferman¹, Amotz Agnon², Regina Katsman¹ and Zvi Ben-Avraham¹**

5 ¹ *The Dr. Moses Strauss Department of Marine Geosciences, Leon H. Charney School of Marine
6 Sciences, University of Haifa, Mt. Carmel, Haifa 3498838, Israel.*

7 ² *The Fredy & Nadine Herrmann Institute of Earth Sciences, The Hebrew University of
8 Jerusalem, Jerusalem 9190401, Israel*

9 Mariana Belferman: mkukuliev@gmail.com (corresponding author)

10 Amotz Agnon: amotz@huji.ac.il

11 Regina Katsman: rkatsman@univ.haifa.ac.il

12 Zvi Ben-Avraham: zviba@post.tau.ac.il

13 **ABSTRACT**

14 Seismicity triggered by water level changes in reservoirs and lakes is usually studied from well-
15 documented contemporary records. Can such triggering be explored on a historical time scale
16 when the data gathered on water level fluctuations in historic lakes and the earthquake catalogs
17 suffer from severe uncertainties? These uncertainties stem from the different nature of the data
18 gathered, methods, and their resolution. In this article, we show a way to considerably improve
19 the correlation between interpolated records of historic water level reconstructions at the Dead
20 Sea and discrete seismicity patterns in the area over the period of the past two millennia. Inspired
21 by the results of our previous study, we carefully revise the historical earthquake catalog in the

22 Dead Sea keeping only events with documented destruction in Jerusalem, the largest historical
23 city in the vicinity of the lake. We then generate an ensemble of random interpolations of water
24 level curves and rank them by correlation with the historical records of seismic stress release. We
25 numerically simulate a synthetic catalog of earthquakes triggered by poroelastic deformations at
26 hypocentral depths. The catalog is produced by a best-fit water level curve and by regional
27 strike-slip tectonic deformations. The earthquakes of this synthetic catalog show an impressive
28 agreement with historic earthquakes documented to damage Jerusalem. We demonstrate for the
29 first time a high correlation between water level changes and the recorded recurrence intervals of
30 historic earthquakes.

31 **KEYWORDS**

32 Seismic recurrence interval; Water level changes; Effective stress; Dead Sea

33 **INTRODUCTION**

34 Triggering of earthquakes by water level changes in lakes and reservoirs has been a focus of
35 seismic investigations around the world (e.g. Simpson et al., 1988; Pandey and Chadha, 2003;
36 Durá-Gómez and Talwani, 2010). Triggering is attributed to a drop in the effective normal stress
37 at a fault, induced by water level change at the overlying lake's bed (Simpson et al., 1988; Durá-
38 Gómez and Talwani, 2010; Hua et al., 2013b; Gupta, 2018). This kind of triggering may be
39 particularly significant for areas with moderate and low tectonic strain accumulations (Pandey and
40 Chadha, 2003; Gupta, 2018), such as the Dead Sea fault in the Middle East (e.g., Masson et al.,
41 2015).

42 Seismic activity due to water level change was observed beneath artificial reservoirs
43 immediately after their first filling (e.g. Simpson et al., 1988; Hua et al., 2013 a). It also appeared
44 after several seasonal filling cycles (Simpson et al., 1988; Talwani, 1997), explained by diffusion
45 of pore pressure to the earthquake's hypocentral depth via the fault (Durá-Gómez and Talwani,
46 2010). The correspondence of this kind of contemporary seismicity to water level change is usually
47 identified based upon real-time data.

48 Alternatively, on a much longer time scale, changing seismic activity may also be associated
49 with water level changes in historic water bodies (e.g., the Dead Sea, since 2 ka, Fig. 1A, in
50 Appendix, which occupies the tectonic depression along the Dead Sea fault). Water level hikes of
51 ~15 m, characteristic for time intervals of centuries to millennia, were analyzed in Belferman et
52 al., (2018) and shown to be able to moderate the seismicity pattern at the Dead Sea fault (Belferman
53 et al., 2018).

54 However, reconstruction of fluctuations in historic lake levels and the concurrent seismicity
55 are both subject to significant uncertainties. They stem from the differing nature of the data
56 gathered on these two phenomena, and thus deserve special consideration. Earthquake dating can
57 be quite precise, and accuracy is verified when different historical sources show consensus
58 (Guidoboni et al., 1994; Guidoboni and Comastri, 2005; Ambraseys, 2009). Assessment of the
59 extent of damage (hence earthquake magnitude), similarly requires such a consensus between the
60 different data sources. Sediment records can help to calibrate the analysis of the historical evidence
61 (Agnon, 2014; Kagan et al., 2011). Such records can be tested by trenching (Wechsler et al., 2014;
62 Marco and Klinger, 2014; Lefevre, 2018). However, in many cases earthquake epicenter can be
63 imprecise or not even known. Consequently, considerable uncertainty pertains to the historical
64 catalog of earthquakes related directly to the Dead Sea.

65 By contrast, historical water level records are quite precise elevation wise, as they are
66 obtained from different points around the lake (Bookman et al., 2004; Migowski et al., 2006).
67 However, water level dating could have an error of about ± 45 yr, as estimated from the radiocarbon
68 dating of shoreline deposits in fan delta outcrops (Bookman et al., 2004). This may underestimate
69 the actual dating uncertainty due to reworking of organic matter, sometimes re-deposited a century
70 or more after equilibration with the atmosphere (Migowski et al., 2004). In addition, the entire past
71 bi-millennial Dead Sea level record is constrained by less than twenty “anchor points” (the data
72 obtained by the dating collected from surveyed paleo-shorelines, Bookman et al., 2004). Therefore,
73 its continuous reconstruction, as suggested in the literature (Migowski et al., 2006; Stern, 2010),
74 usually takes different forms within the acceptable limits dictated by the limnological evidence
75 (Bookman et al., 2004). A challenging uncertainty for our study arises from the interpolations
76 required for periods when the available data does not constrain the water levels.

77 In this article, we take advantage of the correlation between the historic water level
78 reconstructions at the Dead Sea and seismicity patterns in the area over the past two millennia. We
79 demonstrate for the first time that plausible scenarios for the lake level history can fit very well
80 the record of the historic earthquake recurrence intervals (RIs). Based on the correlation between
81 these phenomena, we offer an alternative explanation regarding the triggering of the earthquakes
82 in the area of the Dead Sea.

83 **METHODS**

84 To investigate the relation between an accurate but discrete chronology of earthquakes and
85 the continuous water level (WL) change, we first explore the space of possible WL histories by a
86 statistical approach. We generate an ensemble of WL curves (based on the anchor points
87 (Bookman et al., 2004), while remaining within the limits dictated by climatic and morphological

88 constraints (Bookman et al., 2004; Migowski et al., 2006 and Stern, 2010), by using a random
89 number generator.

90 **A best fit random method of WL curve prediction**

91 The compilation of WL curves of the Dead Sea for the last two millennia from three recent
92 publications (Bookman et al., 2004; Migowski et al., 2006 and Stern 2010) is presented in Figure
93 1A by dashed curves. Generally, the differences between all dashed curves at anchor points is
94 included within an error limit of ± 45 yr as indicated by error bars, with an exception of the anchor
95 point dated to 1400 CE (Bookman et al., 2004) for which Migowski et al. (2006) and Stern (2010)
96 suggested a higher WL. Nevertheless, each hypothetical WL curve is forced to pass through all
97 anchor points according to Bookman et al. (2004) except for one, at around 500 CE. The WL drop
98 around this time, according to Migowski et al. (2006) and Stern (2010), occurred later than was
99 originally suggested by Bookman et al. (2004) (Figure 1A). Because this shift is within the
100 permissible error limits (± 45 yr), this anchor point is shifted to the left (+40 yr). In addition, the
101 WL determined on the curve edges of the studied bi-millennial time interval was defined by
102 additional two anchor points, through which the estimated WL curve passed according to all three
103 references. In total, we have 13 anchor points. Between each pair of points, the trends in the WLs
104 are constrained by the sedimentary facies (Migowski et al., 2006) that specify the edge points of
105 the interval as the extrema for the acceptable WL variation.

106 However, within the largest interval between the anchor points (600 - 1100 CE), the field
107 studies (Migowski et al., 2006; Stern, 2010; Bookman et al., 2004) constrained the WL to be lower
108 than the extrema at the edges of that interval. For this period, the WL was randomly interpolated
109 between higher (e.g., Migowski et al., 2006) and lower (e.g., Stern, 2010) bounds. To maintain a

110 monotony of the WL variation (required by the facies analysis of Migowski et al.), a moving
111 average filtered the random noise between every pair of anchor points. Accounting for the above-
112 mentioned limits, and setting a ten-year step, the model has generated 10 million WL curves for
113 the last bi-millennial interval, using a uniformly distributed random number generator.

114 We test for linear correlation between the recurrence intervals (RIs) of the widely recorded
115 moderate-to-large ($M > 5.5$) historical earthquakes available from the literature (see Table 1 and the
116 text description in Appendix), and the generated WL interpolations. The test is given (as in Figure
117 9 in Belferman et al., 2018) by the value of the Pearson product-moment correlation coefficient,
118 R (Figure 1B). We use this statistic for evaluating the suitability of each randomly interpolated
119 WL curve for our analysis, for identification and elimination of any outliers, and for studying the
120 behavior of the entire ensemble of the curves generated.

121 **The earthquake simulation algorithm**

122 The most suitable WL curve suggested by this correlation (discussed in the results section
123 below), was used to generate a “synthetic” earthquake catalog based on the algorithm described in
124 this section. Effective normal poroelastic stress change due to the WL change is superimposed on
125 the tectonic stress accumulated consistently with the slip rate since the preceding seismic event,
126 and synthetic earthquakes are simulated using a Coulomb failure envelope and a Mohr circle
127 (Jaeger et al., 2009). A vertical outplane strike-slip fault below the lake/reservoir bed is assumed
128 (simulating a Dead Sea fault), embedded in 2D (plain strain) geometry of the upper crust (see
129 Belferman et al., 2018). Tectonic horizontal strike-slip displacements at the fault are approximated
130 by a simple shear approach with no normal strain component.

131 In the poroelastic part of the model, horizontal stress change normal to the strike slip fault
 132 produced by the water level change, is calculated under a uniaxial (vertical) strain condition
 133 (Eq.10b in Belferman et al., 2018), applicable to a post-diffusion stage: i.e., when pore pressure at
 134 hypocentral depth approaches that at the lake's bed. An array of the effective normal stress
 135 changes, $\Delta\sigma'_i$, at the fault, induced by water load change at the lake's bed, p_{s_i} , corresponds to the
 136 array of the WL change, $\Delta h_i (i = 1, 2, \dots 2000)$ over the interpolated water level curve, Figure 1D:

137 1.
$$\Delta\sigma'_i = \frac{1-2\nu}{1-\nu} (\beta - 1) p_{s_i}$$

138 (see Eq. 10b in Belferman et al., 2018). Here β is Biot's coefficient and ν is the Poisson's ratio,
 139 $p_{s_i} = \rho g \Delta h_i$, where ρ is the density of water and g is the acceleration of gravity.

140 A radius and a centre location of the Mohr circle change as a function of tectonic deformations
 141 and water level changes, correspondingly, eventually reaching a failure envelope that simulates an
 142 earthquake. The model uses a Byerlee's law envelope (Byerlee, 1978) to define the residual
 143 strength of a seismogenic zone at the fault immediately after the earthquake (see Belferman et al.,
 144 2018 for more detail). Since the effective stress upon the onset of an earthquake is specified by a
 145 high failure envelope and the effective stress following the slip is given by the Byerlee law, the
 146 model is time-predictable. The stress drop, at least in the nucleation zone, is expected to be
 147 proportional to the recurrence interval.

148 The starting point of the simulations is the date of the first historic earthquake (33CE, see
 149 Table 1 in the Appendix) from the bi-millennial time interval studied. The simulation
 150 incrementally proceeds with time over the WL curve generated (as above) under the accumulating
 151 tectonic stress. After each stress release, the time to the next earthquake, Δt , is calculated from the

152 solution of the Mohr-Coulomb failure criterion for a strike-slip tectonic regime and a WL change,
 153 Δh_i , applicable to the Dead Sea fault (Belferman, et al., 2018):

$$154 \quad 2. \quad (\tau_i - \tau_0)^2 + (\sigma_i - (\sigma_0 + \Delta\sigma'_i))^2 = (R_0 + \Delta\tau_{xy_i})^2$$

$$155 \quad \tau_i = C + \tan(\varphi)\sigma_i$$

156 assuming that $\Delta\tau_{xy_i} = \frac{C \cos(\varphi)}{t_{RI}} \Delta t$ is the tectonic shear stress accumulated consistently with slip-
 157 rate at the strike-slip fault during the period Δt (time passed since the last earthquake), C is
 158 cohesion, φ is an angle of internal friction, σ_0 and τ_0 are the coordinates of the Mohr circle
 159 immediately after the earthquake and R_0 its radius, t_{RI} is the reference RI corresponding to the
 160 minimal WL.

161 For each time step, the algorithm determines whether there is a single solution, or two, or
 162 nil. A case of no solutions means that the Mohr circle is yet to reach the failure envelope, as the
 163 accumulating tectonic stress and the WL increase are still insufficient. The system of Eq. 2 may
 164 have a single solution when the earthquake occurs at the end of some timestep, or two solutions
 165 when the failure criterion is met before the end of the timestep. A case of two solutions is rounded
 166 down to a case of a single solution if a time step (one year) is small compared to the earthquake
 167 RI (several hundreds of years).

168 This solution of Eq.2 yields a RI as a function of the effective normal stress change, $\Delta\sigma'_i$
 169 (Belferman et al., 2018):

$$170 \quad 3. \quad RI = \Delta t = (C + \tan(\varphi)\Delta\sigma'_i) \frac{t_{RI}}{C}$$

171 where t_{RI} is the reference RI corresponds to the minimal WL, C is cohesion, φ is an angle of
172 internal friction. From this formula for RI , an array of earthquake dates is obtained.

173 Substituting Eq.1 into Eq.3, we get a simulated RI as a linear function of WL change with time,
174 Δh_i .

$$175 \quad 4. \quad RI = t_{RI} + \frac{\tan(\varphi)}{C} \frac{1-2\nu}{1-\nu} (\beta - 1) \rho g t_{RI} \Delta h_i$$

176 Coefficients for the simulations were previously determined in Belferman et al. (2018). Note that
177 the cohesion C is not a-priory known hence it is fixed by the empirical correlation between WL
178 and RI for a given lake level history considered. In addition, the slip-rate is set at 5 mm/yr (e.g.
179 Hamiel et al., 2018; Hamiel and Piatibratova, 2019; Masson et al., 2015). The change in WL is
180 calculated relative to its minimal level (415 m bmsl) over the period. A cohesion value, $C =$
181 0.08Mpa and a reference RI , $t_{RI} = 300\text{yr}$, were adjusted numerically for a specific WL curve,
182 providing the average RI of 144 yr over the modelled period of two millennia justified by
183 historical, archaeological, and geological data (Agnon, 2014).

184 **RESULTS**

185 Ten most suitable WL curves (Figure 2) are identified out of the 10M set of WL randomly
186 generated curves (“ensemble”) by the Pearson product-moment correlation test. The values of
187 correlation coefficients, R , for the entire ensemble are distributed normally around $R=0.63$ (Figure
188 1B) with a standard deviation of $\sigma = 0.076$.

189 Three outliers from the thirteen RI s of the widely recorded historic earthquakes (749 CE,
190 1293 CE, 1834 CE in Figure 1) were identified and reevaluated (see the explanation in Appendix).
191 A curve with a highest Pearson coefficient of $R=0.912$ was chosen from the correlation between

192 the RIs of the revised historic catalog and the randomly generated WLs. This correlation can be
193 specified by a linear prediction function

194 5. $RI = -5442 - 14WL$

195 where RI is given in years and WL in meters. In addition, a synthetic earthquake history including
196 14 seismic events was simulated from the best fit randomly interpolated WL curve with R=1
197 specified above. The correlation between the synthetic RIs and WLs (presented in Figure 1C) is:

198 6. $RI = -3840 - 10WL$

199 as expected from the linear dependence suggested by the analytical solution (Eq.4). The dates of
200 the simulated synthetic earthquakes are presented, versus the dates of the historic earthquakes from
201 the literature (Table A1, Appendix) in Figure 1E.

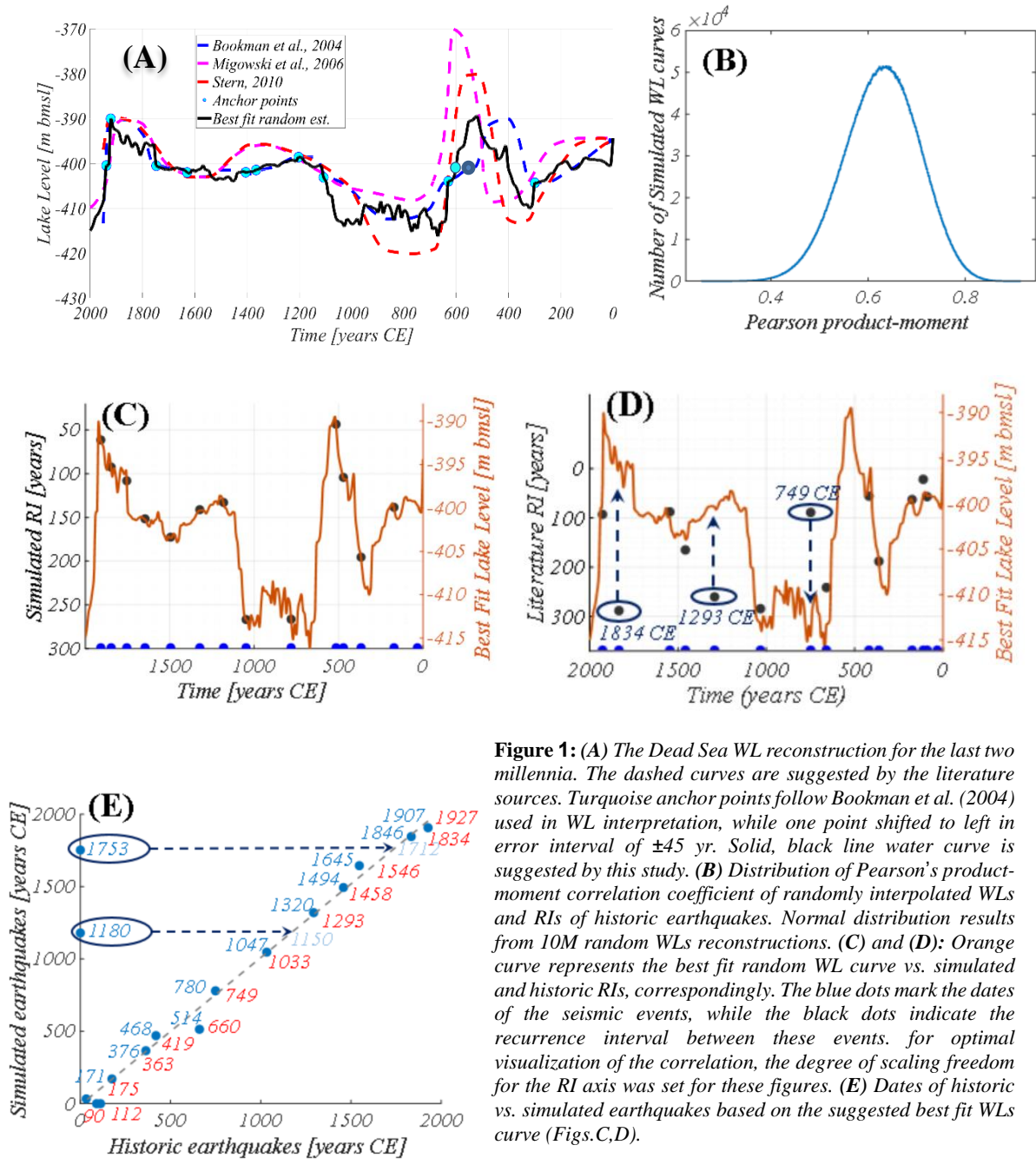


Figure 1: (A) The Dead Sea WL reconstruction for the last two millennia. The dashed curves are suggested by the literature sources. Turquoise anchor points follow Bookman et al. (2004) used in WL interpretation, while one point shifted to left in error interval of ± 45 yr. Solid, black line water curve is suggested by this study. (B) Distribution of Pearson's product-moment correlation coefficient of randomly interpolated WLs and RIs of historic earthquakes. Normal distribution results from 10M random WLs reconstructions. (C) and (D): Orange curve represents the best fit random WL curve vs. simulated and historic RIs, correspondingly. The blue dots mark the dates of the seismic events, while the black dots indicate the recurrence interval between these events. For optimal visualization of the correlation, the degree of scaling freedom for the RI axis was set for these figures. (E) Dates of historic vs. simulated earthquakes based on the suggested best fit WLs curve (Figs. C, D).

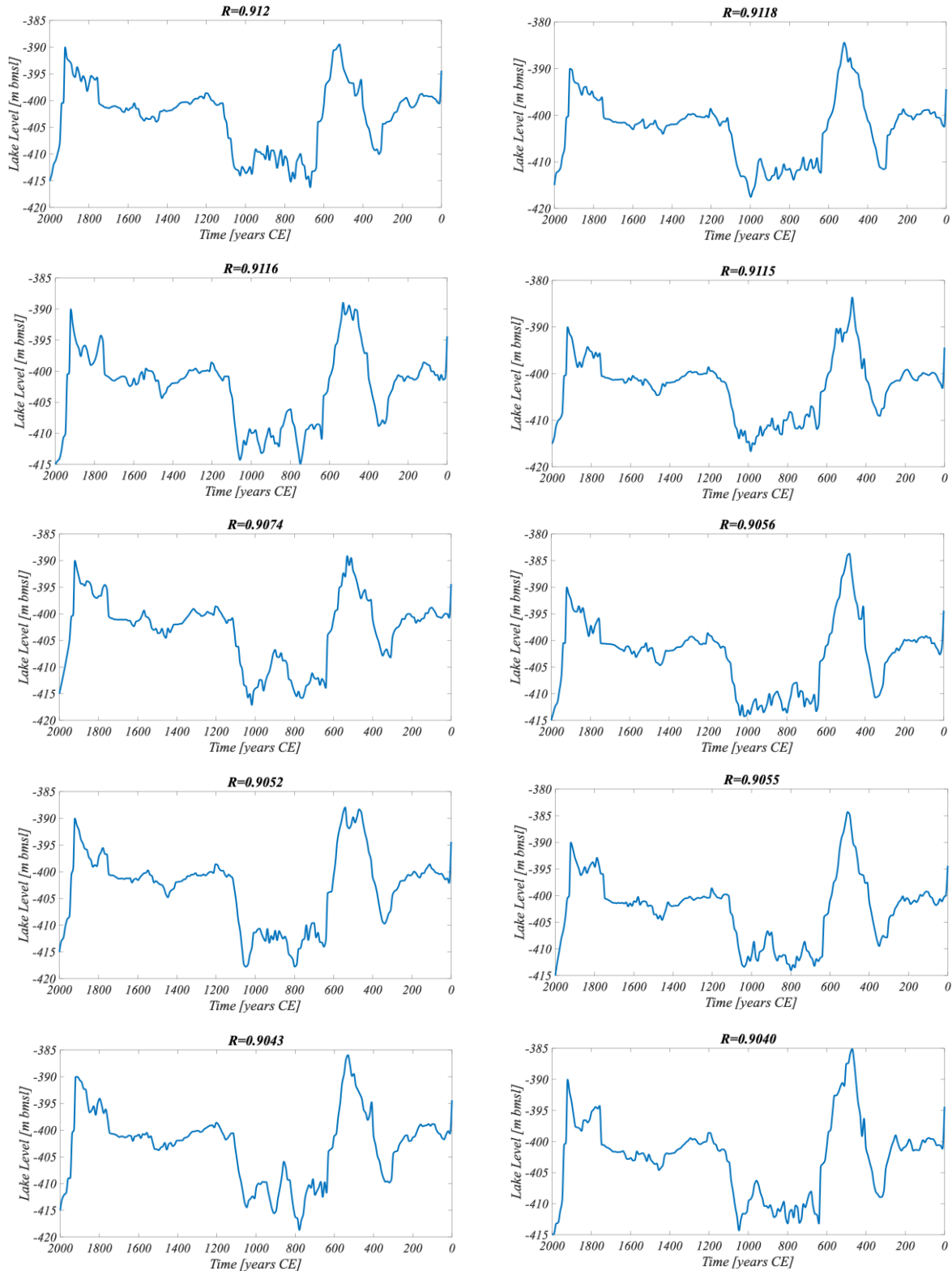


Figure 2: Ten most suitable WLs identified out of the 10M randomly generated by the Pearson product-moment

204 **DISCUSSION**

205 Uncertainties in the WL reconstructions associated with dating and resolution lead to
206 considerable variance in possible interpolations (Figure 1B). A Pearson correlation coefficient test
207 shows that most of the randomly interpolated WL curves give linear correlation with earthquake
208 RIs (indicated by a mean Pearson coefficient of $R=0.63$), excluding the three outliers (Figure 1D)
209 to be discussed below. Figure 2 shows a similar pattern of the WL change for the ten most
210 correlated curves. In all cases, a significant rise in the water level of about 400 CE and 1100 CE is
211 visible and a decrease in the WL around 200 and 600 CE. Also, the maximum level around 500
212 and 1900 CE appears in all ten cases.

213 For simulating synthetic earthquakes triggered by WL change, we use the WL curve that
214 generates the highest correlation with the revised historical catalog ($R = 0.912$). The dates of these
215 simulated synthetic earthquakes are comparable with historical earthquakes (Figure 1E) excluding
216 two events, whose date labels are offset to the y-axis for clarity of presentation (1753 CE, 1180
217 CE). The dates of these synthetic earthquakes might be connected to three outliers from the
218 historical catalog (1834 CE, 1293 CE, 749 CE depicted in Figure 1D) as explained below.

219 The 1180 CE synthetic earthquake (Figure 1E) is comparable to an earthquake in the
220 literature dated by Ben-Menachem (1979) and Amiran et al. (1994) to the mid-12th century (~1150
221 CE). Ambraseys (2009) doubted the precise dating but accepted this mid-12th century estimate.
222 The damaged area of this earthquake spanned Jericho and Jerusalem, and the event could be
223 considered as significant, because it led to the total destruction of two monasteries, one of which
224 is 10 km south of Jerusalem's curtain wall. By admitting the ~1150 CE earthquake to the amended
225 catalog, we reduce the RI of the subsequent earthquake at 1293 CE (Figure 1D) from 260 to 143
226 yrs, thereby bringing this outlier very close to the linear correlation.

227 Our model also generates an earthquake in the 18th century, dated 1753 CE, for which there
228 were no matches in our initial historical catalog (Belferman et al., 2018). However, in Amiran's et
229 al. (1994) catalog an earthquake in 1712 CE is indicated: 'The quake shook the solid houses and
230 ruined three Turkish houses. Felt in Ramle, but not in Jaffa'. Additionally, this earthquake is
231 evidenced by seismites dated to 1700 – 1712 CE from an Ein Gedi site (Migowski et al., 2004).

232 Regarding the modeled 1907 CE event, we note the well documented (although often
233 overlooked) 29 March 1903 CE earthquake (Amiran et al., 1994). This was a moderate but
234 prolonged earthquake: local intensity reached VII in a number of localities distributed outside the
235 rift valley over an area of 140x70 square km (including Jerusalem), whereas the maximum
236 intensity reported in the rift was VII as well (Jericho). We prefer to correlate the modeled 1907
237 event with the stronger 1927 Jericho earthquake that clearly released stress in the Dead Sea (e.g.
238 Shapira, et al., 1993; Avni et al., 2002; Agnon, 2014). This leaves the 1903 unmatched to our
239 model. Perhaps the earthquake ruptured the northern part of the central Jordan Valley, north of the
240 Dead Sea and south of Lake Kinneret (Sea of Galilee).

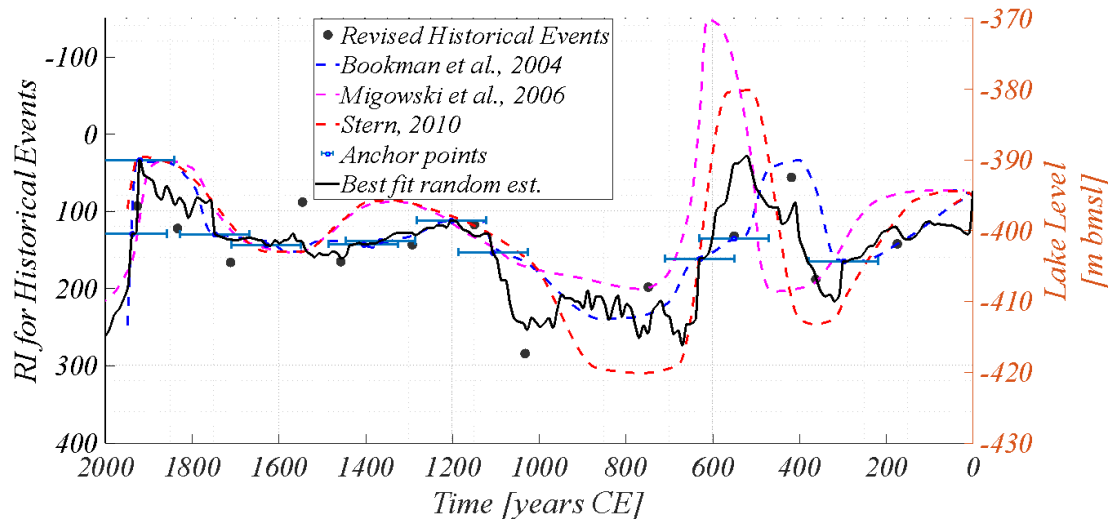
241 Regarding the last outlier from the historical earthquakes dated to 749 CE (or its neighbors
242 747 and 757, Table A1 in the Appendix) (Figure 1D) and corresponding to the simulated 780 CE
243 earthquake (Figure 1E): the simulation generated the preceding earthquake 514 CE associated with
244 the 659/660 CE event from the literature (Table A1 in the Appendix) with a deviation of 146 years.
245 The rupture zone of 659/660 CE event is uncertain, and this earthquake is not necessarily related
246 to stress release at the Dead Sea basin. Alternatively, following Russell (1985), as a result of the
247 551 CE earthquake, a fortress east of the southern Dead Sea and Petra were destroyed. Newer data
248 contradicts the assertion regarding Petra; a failure at the Dead Sea region is still plausible.
249 Replacing the 660 CE earthquake with 551 CE in the catalog changes the RI preceding the 749 CE

250 historical earthquake from 89 to 198, which brings this outlier into a satisfactory linear correlation
251 (Figure 1D).

252 Additionally, it should be emphasized that in the simulation presented in this article, the
253 starting point is, quite arbitrarily, the earthquake of 33CE. This event together with the subsequent
254 earthquakes 90CE and 112CE (not predicted by our model) span a single century where the catalog
255 is nebulous. Each of these events could thus represent the starting point of the simulations or could
256 be omitted at this early and poorly documented interval.

257 Summarizing the above amendments, we add to our catalog of historic events the 551 CE,
258 ~1150 CE, 1712 CE, earthquakes and remove 559/660 CE and 90CE, 112 CE earthquakes (Figure
259 1E). Altogether, we get 14 triggered historic earthquakes.

260 The correlation between the water level and recurrence interval is noticeable for the various
261 variants of the water level curve reconstruction (Figure 3).



262

263 **Figure 3:** *The Dead Sea WL reconstruction for the last two millennia. The dashed curves are suggested by*
264 *the literature. Blue anchor points with an error interval of ± 45 yr follow Bookman et al. (2004). The solid*
265 *black line is the water level curve suggested by this study. The black points represent the RI for revised*
266 *historical events, suggested in this study as being relevant to the Dead Sea area.*

267 The correlation of RI with best fit random estimated curve can be specified by a linear
268 prediction function:

269
$$7. \quad RI = -2483 - 6.5WL$$

270 This linear relationship between WL and RI underscores the previously proposed
271 correlations between these phenomena (in Figure 9 in Belferman et al., 2018).

272 Since the last earthquake (1927CE), the water level in the Dead Sea has continuously
273 decreased at an average annual rate of ~ 1 m/yr. Today the water level is about -440 (m bmsl), thus
274 our prediction function suggests an RI of 377 yr, for such a WL. Alternatively, if the water level
275 in the Dead Sea should remain constant (-440 m bmsl), as intended in some mitigation plans, we
276 would expect the next earthquake at about ~ 2300 yr.

277 This paper stresses that reconstructions of WL curves are not unique and may take various
278 forms under the constraints available (e.g., Figure 1A). However, the correlation with an
279 independent record of RIs of seismic events, assuming that earthquakes are affected by WL hikes,
280 allows deciphering plausible scenarios for WL evolution. Moreover, for cases with the best but
281 not perfect correlation, the deviation might be consistent with a release of elastic energy by smaller
282 earthquakes, which are not accounted for by the deterministic part of our model. We note that
283 smaller earthquakes might rupture dip-slip fault planes, again not accounted for by our simple
284 model.

285 Additionally, as large earthquakes are accompanied by aftershocks, some of the elastic
286 energy is released by them. Moreover, it was shown earlier, in areas where earthquakes caused by
287 artificial reservoirs, how this mechanism influenced by water level change. It was shown that in
288 areas of induced seismicity, earthquakes are not only accompanied by aftershocks but also
289 preceded by foreshocks (Gupta, 2011). The decay curve of this kind of seismicity satisfies criteria
290 for the second class of earthquake sequences by Mogi (1963). The lack of instrumental records of
291 historical earthquakes in our study area, does not allow comparison with this class. The 1995 Gulf
292 of Aqaba earthquake (7.2 Mw), the last instrumentally recorded earthquake, was accompanied by
293 a long period (significant enough for stress release consideration) of aftershocks. The earthquake
294 occurred along the southern part of the plate boundary, which is far enough from the Dead Sea,
295 and most likely is not influenced by the water level change. Following this earthquake, felt
296 aftershocks continued for about two years. At least 50 percent of the total moment associated with
297 these aftershocks was released during the first day after the main shock and over 95 percent in the
298 first 3 months (Baer 2008). In total, the post-seismic moment released during the period of 6
299 months to 2 yr after the Nuweiba earthquake is about 15 percent of the co-seismic moment release
300 (Baer 2008). This earthquake showed that the response of the crust to earthquakes by aftershocks
301 is negligible, as noted for many large earthquakes (e.g., Scholz 1972).

302 For the case of artificial reservoirs, it was shown that for induced seismicity sequences,
303 aftershocks continue for a longer time than for tectonic earthquake sequences (Gupta, 2011).
304 However, because the time scale of RI, the period of aftershocks is insufficient to consider
305 earthquakes from the sequence in our model as separate events. Regarding the time scale presented
306 in our study, when the minimal inter-seismic period is about 50 years, the stress released during
307 post -seismic period can be considered a part of the main shock.

308 The mechanical model used in this article is rather simplistic, where earthquakes release
309 strike-slip loading. The basins around the Dead Sea fault system testify for also an extensional
310 component that could be manifested in co-seismic motion along normal faults. To justify our focus
311 on a single type of fault (strike-slip), we list the following arguments:

312 • The far-field maximal and minimal principal stresses in the Dead Sea region are horizontal
313 (Hofstetter et al., 2007; Palano et al. 2013). This is compatible with a dominance of strike-
314 slip faulting (Anderson, 1951). The tectonic motion at the DSF is characterized
315 predominantly by a left-lateral strike-slip regime with a velocity of ~5 mm/yr along various
316 segments (Garfunkel, 2014; Masson et al.,2015; Sadeh et al., 2012). Large earthquakes that
317 initiate clusters are likely to rupture along the straight ~100 km strike-slip segments
318 (Lyakhovsky et al., 2001). The strike of these segments parallels the relative plate velocity
319 vector and thus can be approximated by a simple shear. Additionally, in the Dead Sea basin,
320 GPS surveys indicate dominance of strike slip loading. Hamiel et al. (2018) show that, on
321 a plate scale, horizontal shear loading dominates the velocity north of the lake. Hamiel and
322 Piatibratova (2019) detected a sub mm/yr component of extension across the southern
323 normal fault bounding the Dead Sea pull apart, yet the strike-slip component across this
324 very fault seems much larger.

325 • Normal, as well as strike-slip faults, similarly react to water level change that contributes
326 to the vertical stress component and pore pressure change. The seismicity induced by
327 surface water level fluctuations and affected by the faulting regime is critically determined
328 by the relative orientations of the three principal stresses (Anderson, 1951). In regions
329 where the vertical compressive stress is not minimal (normal and strike-slip faulting),
330 seismic activity is more sensitive to the effective stress change due to water level change,

331 than in regions where it is minimal (thrust faulting) (Simpson, 1976; Snow, 1982; Roeloffs,
332 1988). This is applicable to a case of reservoirs approximated as “infinite” in horizontal
333 plane (e.g., Wang, 2000), with respect to the fault zone horizontal cross-section. Since we
334 are using a one-dimensional model, such approximation is valid for our study area where
335 the Dead Sea is large enough in a horizontal plane (100 km x 10 km) compared to the
336 thickness of the underlying strike-slip fault (cross-section) located in the central part of the
337 valley.

338 Our results demonstrate that a fairly simple forward model (based on 1D analytical
339 solution, Belferman et al., 2018) achieves a very good correlation between WLs and RIs of
340 moderate-to-strong earthquakes on the Dead Sea fault. Whereas the fault system along the Dead
341 Sea fault is more complicated, three-dimensional modeling of the tectonic motion, coupled to the
342 pore pressure evolution, may give more reliable predictions regarding earthquake ruptures and
343 their chronology. However, based on the relationship between the WL and RI changes presented
344 in this article, with the current anthropogenic decrease in the Dead Sea level (with an average
345 annual rate ~ 1 m / yr), a moderate to severe earthquake will not be triggered by the mechanism
346 discussed here. This article not only presents the existence of a connection between WL and RI,
347 but also provides additional guidance based on this connection, also about the uncertainties
348 regarding the two phenomena separately.

349 **ACKNOWLEDGMENTS**

350 This project was supported by the grants from Ministry of Natural Infrastructures, Energy
351 and Water Resources of Israel # 213-17-002, and GIF- German - Israeli Foundation for Scientific
352 Research and Development # I-1280-301.8. The data for this paper was obtained with analytical
353 and numerical modeling.

354 **REFERENCE**

- 355 Agnon A. 2014. Pre-instrumental earthquakes along the Dead Sea rift. In Dead Sea transform fault
356 system: reviews, edited by Garfunkel, Zvi, Ben-Avraham, Zvi, Kagan, Elisa, 207-261,
357 Springer, Dordrecht. https://doi.org/10.1007/978-94-017-8872-4_8.
- 358 Ambraseys, N. 2009. Earthquakes in the Mediterranean and Middle East: a multidisciplinary study
359 of seismicity up to 1900. Cambridge University Press. doi:
360 <https://doi.org/10.1017/CBO9781139195430>
- 361 Ambraseys, N. N., Melville, C. P. and Adams, R. D. 1994. The Seismicity of Egypt, Arabia and
362 the Red Sea: A Historical Review. Cambridge: Cambridge Univ. Press.
363 <https://doi.org/10.1017/S1356186300007240>
- 364 Amiran, D. H., Arieh, E., and Turcotte, T. 1994. Earthquakes in Israel and adjacent areas:
365 macroscopic observations since 100 B.C.E. *Israel Exploration Journal*, 44, 260– 305.
366 <http://www.jstor.org/stable/27926357>.
- 367 Anderson, E. M. (1951). The dynamics of faulting and dyke formation with applications to Britain.
368 Oliver and Boyd. Avni, R., Bowman, D., Shapira, A. and Nur, A. 2002. Erroneous
369 interpretation of historical documents related to the epicenter of the 1927 Jericho
370 earthquake in the Holy Land. *Journal of seismology*, 6(4), 469-476.
371 <https://doi.org/10.1023/A:1021191824396>
- 372 Baer G., G. J. Funning, G. Shamir, T. J. Wright (2008). The 1995 November 22, Mw 7.2 Gulf of
373 Elat earthquake cycle revisited, *Geophysical Journal International*, 175(3), 1040-
374 1054. <https://doi.org/10.1111/j.1365-246X.2008.03901.x>

375 Belferman, M., Katsman, R. and Agnon, A. 2018. Effect of large-scale surface water level
376 fluctuations on earthquake recurrence interval under strike-slip faulting. *Tectonophysics*,
377 744, 390-402. <https://doi.org/10.1016/j.tecto.2018.06.004>

378 Ben-Menahem, A. 1979. Earthquake catalogue for the Middle East (92 BC-1980 AD). *Boll.*
379 *Geofis. Teor. Appl.*, 21, 245-313.

380 Bookman, R., Enzel, Y., Agnon, A., and Stein, M. 2004. Late Holocene lake levels of the Dead
381 Sea. *Geological Society of America Bulletin* 116, 555-571. <https://doi.org/10.1130/B25286.1>

382 Byerlee, J.D., 1978. Friction of rocks. In: Byerlee, J.D., Wyss, M. (Eds.), *Rock Friction and*
383 *Earthquake Prediction*. Springer, Birkhäuser, Basel, pp. 615–626.
384 <https://doi.org/10.1007/978-3-0348-7182-2>

385 Durá-Gómez, I. and Talwani, P. 2010. Reservoir-induced seismicity associated with the Itoiz
386 Reservoir, Spain: a case study, *Geophysical Journal International*, 181, 343–356.
387 <https://doi.org/10.1111/j.1365-246X.2009.04462.x>

388 Elad, A. 1982. An early arabic source concerning the markets of Jerusalem. *Cathedra*, 24, 31-40.

389 Elad, A., 1992. Two Identical Inscriptions From Jund Filastin From the Reign of the Abbāsīd
390 Caliph, Al-Muqtadir. *Journal of the Economic and Social History of the Orient*, 35(4),
391 301-360. <https://doi.org/10.2307/3632739>

392 Garfunkel, Z., 2014. Lateral motion and deformation along the Dead Sea Transform. In: Garfunkel,
393 Z., Ben-Avraham, Z., Kagan, E. (Eds.), *Dead Sea Transform Fault System: Reviews*. 5.
394 Springer, Dordrecht, pp. 109–150. <http://dx.doi.org/10.1007/978-94-017-8872-4>.

395 Gerber, H., 1998. " Palestine" and Other Territorial Concepts in the 17th Century. *International*
396 *Journal of Middle East Studies*, 30(4), 563-572. <https://www.jstor.org/stable/164341>

397 Guidoboni, E., Comastri, A., and Traina, G. 1994. Catalogue of Ancient Earthquakes in the
398 Mediterranean Area Up to the 10th Century. Rome: Istituto nazionale di geofisica.
399 <https://doi.org/10.1163/182539185X01377>

400 Guidoboni, E. and Comastri, A. 2005. Catalogue of Earthquakes and Tsunamis in the
401 Mediterranean Area from the 11th to the 15th Century. Istituto nazionale di geofisica e
402 vulcanologia. <https://doi.org/10.1515/BYZS.2008.854>

403 Gupta, H., K., 2018, Reservoir triggered seismicity (RTS) at Koyna, India, over the past 50
404 yrs. *Bulletin of the Seismological Society of America* 108.5B: 2907-2918.
405 <https://doi.org/10.1785/0120180019>

406 Hamiel, Y., Masson, F., Piatibratova, O., & Mizrahi, Y. (2018). GPS measurements of crustal
407 deformation across the southern Arava Valley section of the Dead Sea Fault and
408 implications to regional seismic hazard assessment. *Tectonophysics*, 724, 171-178.
409 <https://doi.org/10.1016/j.tecto.2018.01.016>

410 Hamiel, Y., & Piatibratova, O. (2019). Style and distribution of slip at the margin of a pull-apart
411 structure: Geodetic investigation of the Southern Dead Sea Basin. *Journal of Geophysical*
412 *Research: Solid Earth*, 124(11), 12023-12033. <https://doi.org/10.1029/2019JB018456>

413 Hofstetter, R., Klinger, Y., Amrat, A. Q., Rivera, L., & Dorbath, L. (2007). Stress tensor and focal
414 mechanisms along the Dead Sea fault and related structural elements based on
415 seismological data. *Tectonophysics*, 429(3-4), 165-181.
416 <https://doi.org/10.1016/j.tecto.2006.03.010>

- 417 Hua, W., Chen, Z. and Zheng, S., 2013a. Source parameters and scaling relations for reservoir
418 induced seismicity in the Longtan reservoir area. *Pure Appl. Geophys.* 170, 767–783.
419 <https://doi.org/10.1007/s00024-012-0459-7>
- 420 Hua, W., Chen, Z., Zheng, S., and Yan, C., 2013b. Reservoir-induced seismicity in the Longtan
421 reservoir, southwestern China. *J. Seismol.* 17 (2), 667–681.
422 <https://doi.org/10.1007/s10950-012-9345-0>
- 423 Hough S. E. and Avni R., 2011. The 1170 and 1202 CE Dead Sea Rift earthquakes and long-term
424 magnitude distribution of the Dead Sea Fault Zone, *Isr. J. Earth Sci.*, 58, 295–308.
425 <https://doi.org/10.1560/IJES.58.3-4.295>
- 426 Jaeger, J. C., Cook, N. G., & Zimmerman, R. (2009). *Fundamentals of rock mechanics*. John Wiley
427 and Sons.
- 428 Kagan, E., Stein, M., Agnon, A., and Neumann, F. 2011. Intrabasin paleoearthquake and
429 quiescence correlation of the late Holocene Dead Sea. *Journal of Geophysical Research:*
430 *Solid Earth*, 116(B4). <https://doi.org/10.1029/2010JB007452>
- 431 Ken-Tor, R., Agnon, A., Enzel, Y., Stein, M., Marco, S., and Negendank, J. F. 2001. High-
432 resolution geological record of historic earthquakes in the Dead Sea basin. *Journal of*
433 *Geophysical Research-Solid Earth*, 106, 2221-2234.
434 <https://doi.org/10.1029/2000JB900313>
- 435 Langgut, D., Yannai, E., Taxel, I., Agnon, A. and Marco, S., 2015. Resolving a historical
436 earthquake date at Tel Yavneh (central Israel) using pollen seasonality. *Palynology*, 40(2),
437 145-159. <https://doi.org/10.1080/01916122.2015.1035405>

438 Lefevre, M., Klinger, Y., Al-Qaryouti, M., Le Béon, M. and Moumani, K., 2018. Slip deficit and
439 temporal clustering along the Dead Sea fault from paleoseismological investigations. *Sci.*
440 *Rep.* 8 (1), 4511. <https://doi.org/10.1038/s41598-018-22627-9>

441 Lyakhovsky, V., Ben-Zion, Y., Agnon, A., 2001. Earthquake cycle, fault zones, and seismicity
442 patterns in a rheologically layered lithosphere. *J. Geophys. Res. Solid Earth* 106 (B3),
443 4103–4120.

444 Marco, S., Stein, M., Agnon, A., and Ron, H. 1996. Long-term earthquake clustering: A 50,000-
445 year paleoseismic record in the Dead Sea Graben. *Journal of Geophysical Research: Solid*
446 *Earth*, 101(B3), 6179-6191. <https://doi.org/10.1029/95JB01587>

447 Masson, F., Hamiel, Y., Agnon, A., Klinger, Y. and Deprez, A., 2015. Variable behavior of the
448 Dead Sea Fault along the southern Arava segment from GPS measurements. *comptes*
449 *rendus geoscience*, 347(4), pp.161-169. <https://doi.org/10.1016/j.crte.2014.11.001>

450 Migowski, C., Agnon, A., Bookman, R., Negendank, J. F., and Stein, M. 2004. Recurrence pattern
451 of Holocene earthquakes along the Dead Sea transform revealed by varve-counting and
452 radiocarbon dating of lacustrine sediments. *Earth and Planetary Science Letters*, 222, 301–
453 314. <https://doi.org/10.1016/j.epsl.2004.02.015>

454 Migowski, C., Stein, M., Prasad, S., Negendank, J. F. W., and Agnon, A. 2006. Holocene climate
455 variability and cultural evolution in the Near East from the Dead Sea sedimentary record.
456 *Quaternary Research*, 66(3), 421-431. <https://doi.org/10.1016/j.yqres.2006.06.010>

457 Palano, M., Imprescia, P., & Gresta, S. (2013). Current stress and strain-rate fields across the Dead
458 Sea Fault System: Constraints from seismological data and GPS observations. *Earth and*
459 *Planetary Science Letters*, 369, 305-316. <https://doi.org/10.1016/j.epsl.2013.03.043>

460 Pandey, A.P. and Chadha, R.K., 2003. Surface loading and triggered earthquakes in the Koyna–
461 Warna region, western India. *Phys. Earth Planet. Inter.* 139 (3–4), 207–223.
462 <http://dx.doi.org/10.1016/j.pepi.2003.08.003>

463 Parker, S.T., 1982. Preliminary Report on the 1980 Season of the Central " Limes Arabicus"
464 Project. *Bulletin of the American Schools of Oriental Research*, 247(1), pp.1-26.
465 <https://www.journals.uchicago.edu/doi/10.2307/1356476>

466 Rao, N. P., & Shashidhar, D. (2016). Periodic variation of stress field in the Koyna–Warna
467 reservoir triggered seismic zone inferred from focal mechanism
468 studies. *Tectonophysics*, 679, 29-40. <https://doi.org/10.1016/j.tecto.2016.04.036>

469 Russell, K. W., 1985. The earthquake chronology of Palestine and northwest Arabia from the 2nd
470 through the mid-8th century AD. *Bulletin of the American Schools of Oriental*
471 *Research*, 260(1), 37-59. <https://doi.org/10.2307/1356863>

472 Sadeh, M., Hamiel, Y., Ziv, A., Bock, Y., Fang, P., Wdowinski, S., 2012. Crustal deformation
473 along the Dead Sea Transform and the Carmel Fault inferred from 12 years of GPS
474 measurements. *J. Geophys. Res. Solid Earth* 117, B08410.
475 <http://dx.doi.org/10.1029/2012JB009241>.

476 Scholz, C. H. (1972). Crustal movements in tectonic areas. *Tectonophysics*, 14(3-4), 201-217.
477 [https://doi.org/10.1016/0040-1951\(72\)90069-8](https://doi.org/10.1016/0040-1951(72)90069-8)

478 Shapira, A., Avni, R., and Nur, A. 1993. A new estimate for the epicenter of the Jericho earthquake
479 of 11 July 1927. *Isr. J. Earth Sci*, 42(2), 93-96.

480 Simpson, D. W. (1976). Seismicity changes associated with reservoir loading. *Engineering*
481 *Geology*, 10(2-4), 123-150. [https://doi.org/10.1016/0013-7952\(76\)90016-8](https://doi.org/10.1016/0013-7952(76)90016-8)

482 Simpson, D. W., Leith, W., and Scholz, C. 1988. Two types of reservoir-induced seismicity.
483 *Bulletin of the Seismological Society of America*, 78, 2025–2040.

484 Snow, D. T. (1982). Hydrogeology of induced seismicity and tectonism: Case histories of Kariba
485 and Koyna. *Geological Society of America Special Papers*, 189, 317-360.
486 <https://doi.org/10.1130/SPE189-p317>

487 Stern, O. 2010. Geochemistry, Hydrology and Paleo-Hydrology of Ein Qedem Spring System;
488 Report GSI/17/2010; Geological Survey of Israel: Jerusalem, Israel, 2010; p. 91. (In
489 Hebrew)

490 Talwani, P., 1997. On the nature of reservoir-induced seismicity. *Pure Appl. Geophys.* 150, 473–
491 492. https://doi.org/10.1007/978-3-0348-8814-1_8

492 Wang, H., 2000. *Theory of Linear Poroelasticity With Applications to Geomechanics and*
493 *Hydrogeology*. University Press, Princeton.

494 Wechsler, N., Rockwell, T. K., Klinger, Y., Štěpančíková, P., Kanari, M., Marco, S., & Agnon, A.
495 (2014). A paleoseismic record of earthquakes for the Dead Sea transform fault between the
496 first and seventh centuries CE: Nonperiodic behavior of a plate boundary fault. *Bulletin of*
497 *the Seismological Society of America*, 104(3), 1329-1347. <https://doi.org/10.1785/0120130304>

498 Williams, J. B., Schwab, M. J., & Brauer, A. 2012. An early first-century earthquake in the Dead
499 Sea. *International Geology Review*, 54(10), 1219-1228.
500 <https://doi.org/10.1080/00206814.2011.639996>

501
502
503
504
505
506
507
508
509
510
511
512
513
514
515
516
517
518
519
520
521

Appendix: The earthquake history of the Dead Sea environs

Numerous publications list earthquakes that hit the Dead Sea and its surroundings during the last two millennia (e.g. Agnon, 2014; Ambraseys et al., 1994; Ambraseys, 2009; Amiran et al., 1994; Guidoboni et al., 1994, Guidoboni and Comastri, 2005). In Belferman et al. (2018) we adopted from the scores of listed events only the most destructive ones, typically causing local intensities of VII or higher in Jerusalem. For a minimal epicentral distance of 30 km, this would translate to a magnitude of ~5.7 or higher (according to the attenuation relation of Hough and Avni, 2011). Table A1 lists the Dead Sea earthquakes considered for stress release across the Dead Sea basin during the last two millennia. We used two criteria: noticeable damage in fortified Jerusalem, and seismites in the northern Dead Sea. Our simple model simulates an earthquake time series, given a water level curve. Eleven events from this time series correlate with events of magnitude ~6 or more in the historic record. Yet, the model generates four events that are not included in our original catalog. On the other hand, a single event (~660 CE) listed in Belferman et al. (2018) has no counterpart in the simulations despite a wide range of level curves tested. All these curves are generated by a random number generator, subject to constraints from field data. We first discuss the four events required by the simulations one by one. Then we review the ~660 CE event along with other historic events that were left out already in Belferman et al. (2018).

522 The earthquakes in Table 1 are classified according to the level of acceptance for being destructive
523 in Jerusalem. The nine events of **Class C** are all consensual, also used by Belferman et al.(2018).
524 These events appear in all catalogs and lists, and need no further discussion. The six events of
525 **Class A** are debated events, accepted in the present study. All earthquakes in this class are selected
526 by simultaneously satisfying two criteria: (1) The acceptance regularizes the relation between
527 recurrence intervals and lake level; (2) They are corroborated by evidence from seismites in the
528 northern basin of the Dead Sea (Ein Feshkha and Ein Gedi sites, Fig.A1corroborate).

529 We chose the year **33 CE** to start our simulations. While this earthquake did not cause a widespread
530 damage, it was recorded in all three seismite sites (Kagan et al., 2011), with a maximum of decade
531 uncertainty based on dating by counting lamina under the microscope (Migowski et al., 2004;
532 Williams et al., 2012).

533 The second entry in Table A1, **~100 CE**, refers to two decades of unrest. Migowski et al. (2004)
534 identified a pair of seismites around 90 CE and 112 CE in the 'Ein Gedi Core. The corresponding
535 sequences in Ein Feshkha and Ze'elim Creek are laminates, attesting to quiescence. A historical
536 hiatus between the Roman demolition of Jerusalem and the erection of Ilya Capitolina in its stead
537 (70-130 CE) preclude historical evidence. Although damage to the Masada fortress has been
538 assigned to an earthquake **1712 CE**.

539 Table A2 lists ten earthquakes that have been reported to damage around Jerusalem but are not
540 required by our simulations. The seven events of **Class R** are the debated events, rejected here
541 after discussion. The three **Class S** events were skipped altogether in that compilation of
542 Ambraseys (2009).

543 Of the seven Class R events, the 7 June **659 CE** earthquake was accepted by us in Belferman et al.
544 (2018). The earthquake has been associated with destruction of the Euthymius monastery 10 km

545 east of Jerusalem, but no damage in the town of Jerusalem has been unequivocally reported
546 (Ambraseys, 2009). In Belferman et al. (2018) we included this event in the catalog of Dead Sea
547 earthquakes, as Langgut et al. (2015) have located it on the center of the Jordan Valley segment of
548 the transform (Figure A1). However, this interpretation neglected the possibility that the rupture
549 could have been outside the hydrological effect of the Dead Sea basin. One of the lessons of our
550 numerous simulations is that our model would not support triggering of this earthquake shortly
551 (less than a century) before the mid-8th century crisis, when lake levels were dropping to the lowest
552 point in the studied period (420 m bsl, Figure 1a). When rejecting the 659 CE event, the 419 CE
553 earthquake is the one preceding the mid-8th century crisis; the three century recurrence interval
554 fits well the low lake level.

555 **1016 CE:** The collapse of the Dome of the Rock was not explicitly attributed to an earthquake by
556 the original sources, who found it enigmatic as well (Ambraseys, 2009).

557 **1644 CE:** Ambraseys (2009) quoted a late Arab author, al-Umari, who reported collapse of houses
558 and deaths of five persons in “the town of Filistin”. While Ambraseys has interpreted it probably
559 to Jerusalem, it might refer to al-Ramla, the historical capital of the classical Filistin District, as in
560 “al-Ramla, Madinat Filastin” (Elad, 1992, p335). Or, it is a mistranslation of “Bilad Filistin” which
561 at that time started refer to the entire Holy Land district, without specifying a town (Gerber, 1998).
562 Jerusalem, at that time, was called Bayt el Maqdis or, as nowadays, al-Quds. The only report of an
563 earthquake in Jerusalem around 1644 mentions horror but no structural damage - the 1643 CE
564 event that Ambraseys (2009) tends to equate with the 1644 CE event. A seismite in Ein Gedi core
565 can be correlated with this event (Migowski et al., 2004, Table 2, entry 6). Migowski et al. (2004)
566 have identified the seismite with the 1656 earthquake that was felt in Palestine; Ambraseys’ (2009)
567 interpretation was not yet available for them.

568 **1656 CE:** This event was strong in Tripoli and only felt in Palestine. Migowski et al. (2004)
569 correlated it to a seismite based on deposition rates (no lamina counting for that interval). Given
570 the 1644 CE entry of Ambraseys (2009), this interpretation should be revised, and the 1656 CE
571 earthquake is not to be associated with any local rupture in the Dead Sea.

572
573
574
575

Table A1: A catalog of earthquakes that could potentially damage Jerusalem. The classes denote the level of acceptance of damage to Jerusalem among the researchers: C - consensual; B - accepted by Belferman et al., 2018; A - amended here; R - rejected here.

Year CE or Century (marked C)	Class	Seismite correl. by site			Reference	Comments
		Z E †	E G ^Y	E F ^o		
33	B	+	+	+	MI,K&,W&	Identified in all three seismites sites, varve-counted to 31 BCE
100~	B	-	2	-	MI,AM	Seismites ~90 and ~112; questionable archaeological evidence
~175	B	-	+	-	MI	A seismite; no historic or archeological support
363	C	-	-	+	K&,A&	A seiche in the Dead Sea, a seismite at EF° (north Dead Sea)
419	C	+	+	+	KT/MI/K&	
551	A	+	+	+	PA,AM	
747/9,757	C	+	+	+	KT/MI/K&	
1033	C	?	+	+	KT/MI/K&	
~1150	A	+	-	/	AM,K&	I ₀ IX - Mar Elias (& Qasr al-Yahud) monasteries demolished
1293	C	+	+	+	K&	
1458	C	+	+	h	MI	
1546	C	/	+	i	MI	
1712	A	/	+	a	MI	A& / I ₀ VII - “ruined three Turkish houses in Jerusalem”
1834	C	+	+	t	KT,MI	
1903	R	m	m	u	A&,AM	I ₀ VII Mt. of Olives; several shocks, I ₀ up to VII over a large area
1927	C	+	+	s	KT,MI	AV / I ₀ VII-VIII in and around Jerusalem (I ₀ 7.8 by GMPE)

576
577
578
579
580

581
582
583

Table A2: Events listed in some catalogs and subsequently skipped (Class S) or declined (Class D) by Ambraseys (2009), or rejected (Class R) in the present study.

Year CE	C l a s s	Seismite correl. by site			Reference	Comments
		Z E †	E G ^Y	E F °		
~659	R	-	+	+	L&,AM	Jordan Valley, possibly over 65 km NE of Jerusalem
808	S	/	-	?	A&	
1016	D	?	?	?	AM,A&	Damage to the Dome of Rock, no specific reference to shaking
1042	S	-	+	-	BM	Syria, off the Dead Sea transform
1060	S	/	-	+	A&,SB	The roof of Al-Aqsa collapsed
1063	R				A&,AM,SB	Syrian littoral
1068	D	+	+	+	AM	Neither of the two events can be associated with the Dead Sea
1105	D	?	?	?	A&,AM	“Strong” but “no damage recorded in the sources”
1114	D	+	+	?	A&,AM	1114 - no damage around the city, a swarm, Kingdom’s north
~1117	R	+		?	A&,AM	
1557	R				Am	Collapse in Jerusalem: a gun foundry, a forgery, an oven
1644	R	h	+*	h	Am	Some damage and death toll in Palestine, likely Seismite 6 of MI
1656	R	h	-	h	A&,AM,SB	Tripoli VII, Palestine IV, MI misidentified with Seismite 6
1817	R				AM	Two churches damaged in Jerusalem, Holy Sepulchre affected
1870	S	?	-	h	AM	Mediterranean source

584 Abbreviations and notes:

585 †ZE - Ze' elim Creek; ‡EG - Ein Gedi core; °EF - Ein-Feshkha Nature Reserve

586 AM: Ambraseys, 2009; A&: Amiran et al., 1994; K&: Kagan et al., 2011; L&: Langgut et al.

587 2015; KT: Ken-Tor et al., 2004; MI: Migowski et al., 2004; PA: Parker, 1982; W&: Williams et

588 al., 2012.

589

590

591

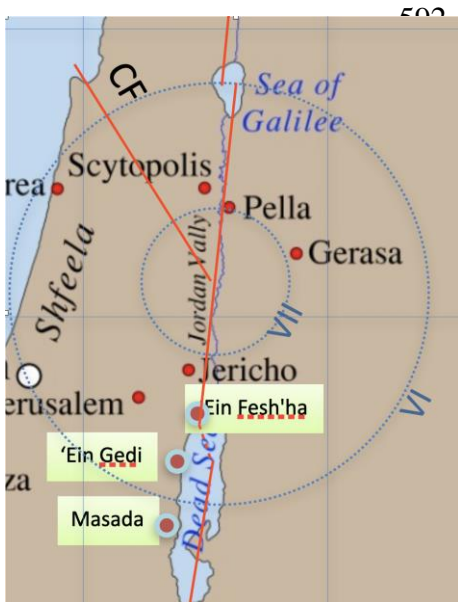


Figure A1: A map showing the epicenter reconstructed by Langgut et al. (2015) for the 659/660 mainshock.